Since January 2020 Elsevier has created a COVID-19 resource centre with free information in English and Mandarin on the novel coronavirus COVID-19. The COVID-19 resource centre is hosted on Elsevier Connect, the company's public news and information website.

Talanta 259 (2023) 124490

Contents lists available at ScienceDirect

Talanta

journal homepage: www.elsevier.com/locate/talanta

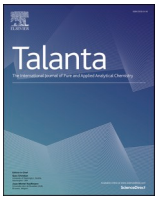

An electrochemical PNA-based sensor for the detection of the SARS-CoV-2 RdRP by using surface-initiated-reversible-addition−fragmentation-chain-transfer polymerization technique

Mahmoud Amouzadeh Tabrizi

Electronic Technology Department, Universidad Carlos III de Madrid, 28911, Leganés, Spain

A R T I C L E I N F O

Handling Editor: J.-M. Kauffmann

Kewords:
Electrochemical biosensor
Reduced graphene oxide-gold nanocomposite
SI-RAFT
SARS-CoV-2

A B S T R A C T

Coronavirus disease 2019 is one of the global health problems. Herein, a highly sensitive electrochemical biosensor has been designed to detect the RNA-dependent RNA polymerase (RdRP) of the severe acute respiratory syndrome coronavirus-2 (SARS-CoV-2) (SARS-CoV-2 RdRP). Herein, the surface-initiated reversible-addition−fragmentation-chain-transfer polymerization was used to amplify the electrochemical signal. To do that, the thiol-terminated peptide nucleic acid (PNA) probes were first immobilized on the surface of a screen-printed electrode modified with reduced graphene oxide-gold nanocomposite and then the fixed concentration of the SARS-CoV-2 RdRP was added to the electrode surface to interact with PNA probes. Subsequently, the Zr^{4+} ions were added to interact with the phosphate groups of the SARS-CoV-2 RdRP. It allowed us to polymerase the ferrocenylmethyl methacrylate (FcMMA) and 4-cyano-4-(phenylcarbonothioylthio)-pentanoic acid on the SARS-CoV-2 RdRP chain. Since the poly-FcMMA has an electrochemical signal, the response of the PNA-based sensor to SARS-CoV-2 RdRP was increased in the range of 5–500 aM. The limit of detection was calculated to be 0.8 aM which is lower than the previous sensor for SARS-CoV-2 RdRP detection. The proposed PNA-based sensor showed high selectivity to the SARS-CoV-2 RdRP in the presence of the gene fragments of influenza A and Middle East respiratory syndrome coronavirus.

1. Introduction

Nowadays, artificial receptors (ARs) have been used for the fabrication of the sensor widely [1]. They have several advantages such as low cost, easy to functionalize and ease of integration with various transducers able to detect various targets like metal ions [2], gene fragments [3], tumor markers [4], and cells [5] with high selectivity. Peptide nucleic acid (PNA) [6], deoxyribonucleic acid (DNA), and ribonucleic acid (RNA) [7] are the common ARs that have integrated with the electrochemical transducer. Unlike DNA and RNA, the PNA backbone carries no charges. It paves the way to use the surface-initiated reversible-addition−fragmentation-chain-transfer (SI-RAFT) polymerization method to increase the sensitivity of the sensor to the DNA or RNA-based targets. This method was used for the detection of the gene fragments at the trace level [8–10]. Because a poly-probe is generated on the surface of each gene fragment and the signal gets amplified. In this method, first, a highly positively charged ion like zirconium ions (Zr^{4+}) interacts with the negatively charged phosphate groups of the gene fragments (DNA or RNA) in the PNA/DNA (RNA) double strand. After that, the 4-cyano-4-(phenylcarbonothioylthio)-pentanoic acid (CPAD) which has negatively charged molecules and can interact with Zr^{4+} ions is added to the reaction cell. CPAD is an SI-RAFT agent that helps polymerize the molecules containing acrylate groups like ferrocenylmethyl methacrylate (FcMMA) [11] and fluorescein-o-acrylate [12]. Since the ferrocene is an electrochemical probe, and PNA can integrate with the electrochemical transducer, the SI-RAFT strategy for the amplification of the electrochemical signal can be used for the gene fragments of dangerous microorganisms such as viruses. Since the severe acute respiratory syndrome coronavirus-2 (SARS-CoV-2) causes coronavirus disease 2019 (COVID-19), I decided to fabricate an electrochemical sensor to detect the RNA-dependent RNA polymerase (RdRp) of SARS-CoV-2 (SARS-CoV-2 RdRP). The SARS-CoV-2 RdRP concentration has been detected by several research groups [13,14] but none of them could detect it at the attomolar level. In this research work, the surface of the carbon screen-printed electrode (CSPE) was modified with the reduced graphene oxide decorated with gold ($rGO\text{-}Au_{nano}$) that was synthesized by our proposed method in the past [15]. Then the thiol-terminated PNA probe was attached on the surface of the

E-mail addresses: mamouzad@ing.uc3m.es, mahmoud.tabrizi@gmail.com.

https://doi.org/10.1016/j.talanta.2023.124490
Received 30 January 2023; Received in revised form 16 March 2023; Accepted 26 March 2023
Available online 29 March 2023

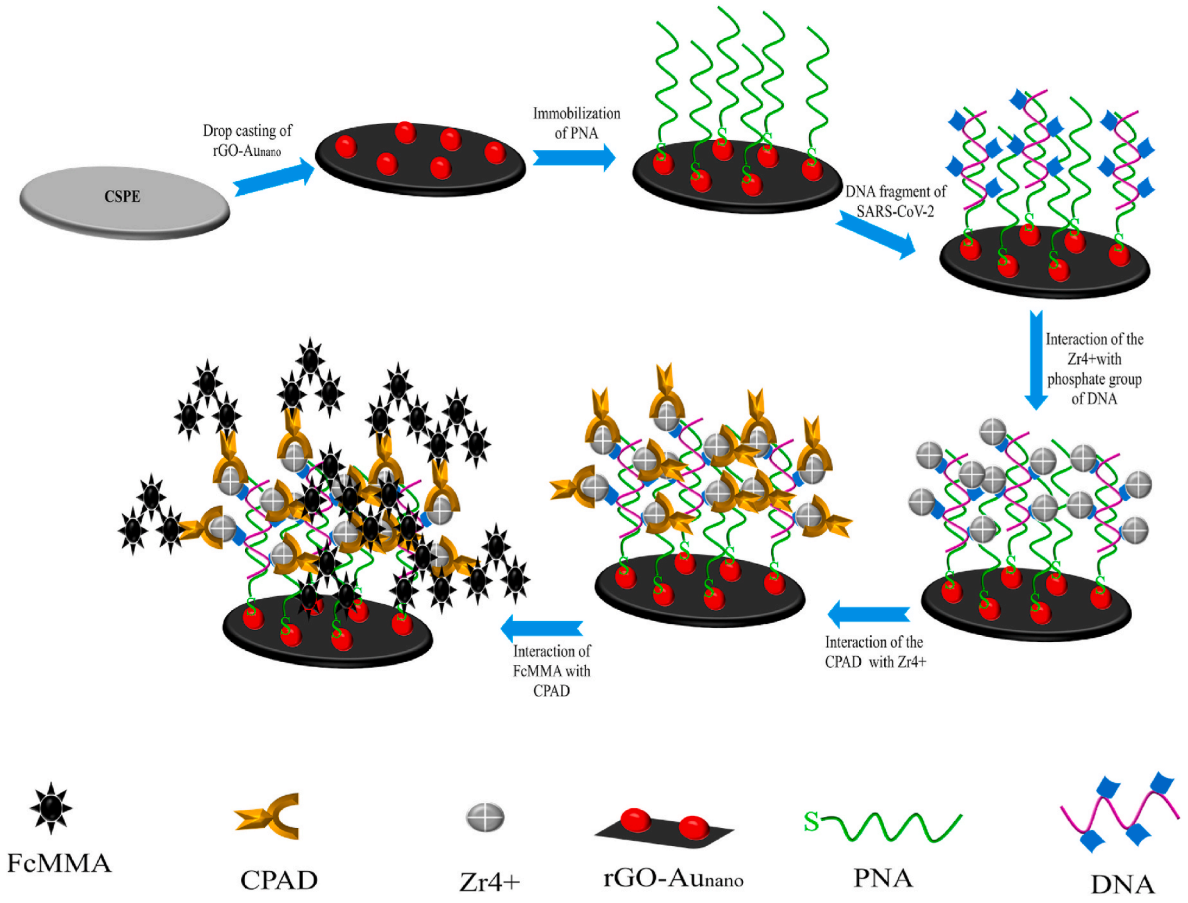

Fig. 1. Scheme of the process of fabrication and the response of the proposed PNA-based sensor.

CSPE/rGO-Au_{nano} via the Au-thiol (Au–S) covalent bond. After adding the SARS-CoV-2 RdRP gene fragment, the SI-RAFT strategy was applied to amplify the electrochemical signal. The PNA-based sensor (CSPE/r-GO-Au_{nano}/PNA) had a selectivity to the SARS-CoV-2 RdRP in the presence of the gene fragments of influenza A (H1N1) and Middle East respiratory syndrome coronavirus (MERS-CoV) and high stability up to 20 days.

2. Experimental section

2.1. Reagents and chemicals

The thiol-terminated PNA probe and the short gene fragments with the following sequences were obtained from biomers.net (Germany):

Thiol-terminated PNA probe: (5′-thiotic acid–8-Amino-3,6-dioxaoctanoic acid GCATCTCCTGATGAGGTTCCACCTG-3′), SARS-CoV-2 RdRP: 5′-CAGGT GGAAC CTCATCAGGA GATGC-3′ [13],

H1N1: 5′-CTAGTACTGTGTCTACACAGTGTC-3′ [16],

MERS-CoV: 5′-CGATTATGTGAAGAG-3′ [6].

Potassium chloride (KCl), calcium chloride, sodium chloride (NaCl), sodium nitrate ($NaNO_3$), magnesium chloride ($MgCl_2$), and sodium dihydrogen phosphate (NaH_2PO_4) were purchased from Cymit Química (Spain). 1-Hexanethiol (HT), graphite powder, zirconium dichloride oxide octahydrate ($ZrOCl_2$), ferrocenylmethyl methacrylate (FcMMA), 4-cyano-4-(phenylcarbonothioylthio)-pentanoic acid (CPAD), 2,2′-azo-bis [2-(2-imidazolin- 2-yl)propane] dihydrochloride (AIPH), ethanol (EtOH), *N*,N-dimethylformamide (DMF), sodium tetrachloroaurate (III) dehydrate ($NaAuCl_4$), potassium permanganate ($KMnO_4$), hydrochloric acid (HCl), potassium hydroxide (KOH), hydrogen peroxide (H_2O_2), (30%), potassium ferricyanide (K_3 [$Fe(CN)_6$]), potassium ferrocyanide (K_4 [$Fe(CN)_6$]), from Sigma-Merck (USA). Disposable well cells and carbon screen printed electrodes (CSPE, Ref 110) were purchased from Metrohm-DropSens (Spain).

2.2. The fabrication of the PNA-based sensor

The surface of a CSPE was cleaned with running PBS (0.1 M, pH 7.4). After that, the surface dried with airflow. Then 5 μL of the rGO-Au_{nano} solution that was synthesized by in my group [15] cast on the surface of a CSPE and allowed dry at room temperature. The CSPE/rGO-Au_{nano} was washed with 0.1 M PBS. A disposable well cell for the CSPE was attached to the electrode to isolate the electrodes (Fig. S1) and consequently, 300 μL PNA (0.1 mM, 0.1 M PBS, pH 7.4) was dropped inside the disposable well cell. The electrode containing the PNA solution was put in a box and kept at room temperature (37 °C) for 24 h. During this time, the thiol-terminated PNA probes attached on the surface of CSPE/rGO-Au_{nano} via the covalent bond between the thiol terminals (S–S) and Au_{nano}. To avoid non-specific binding, 100 μL of 100 μM HT was added to the electrode at a temperature for half an hour to block the rest of the active sites on the gold nanoparticles. After this period, the PNA-based sensor (CSPE/rGO-Au_{nano}/PNA) was washed with 0.1 M PBS and stored in a fridge (4 °C) when not in use. The surface coverage (Γ) of the PNA probes was found to be 178 pmol cm^{-2}. The calculation was based on the integration of the faradaic charge at −0.87 V that is related to the reduction of the gold-thiolate layer bounds (Au–S_2-PNA) in N_2 saturated alkaline solution (pH > 11):

$PNA - S_2 - Au + 2e^- \rightarrow Au(0) + PNA - S_2^{2-}$ [17,18]. The details were mentioned in the supplementary data (Fig.S 2-3 and Tables S1–2). The biosensor (CSPE/rGO-Au_{nano}/PNA) was fabricated according to a procedure described in a previous literature [8].

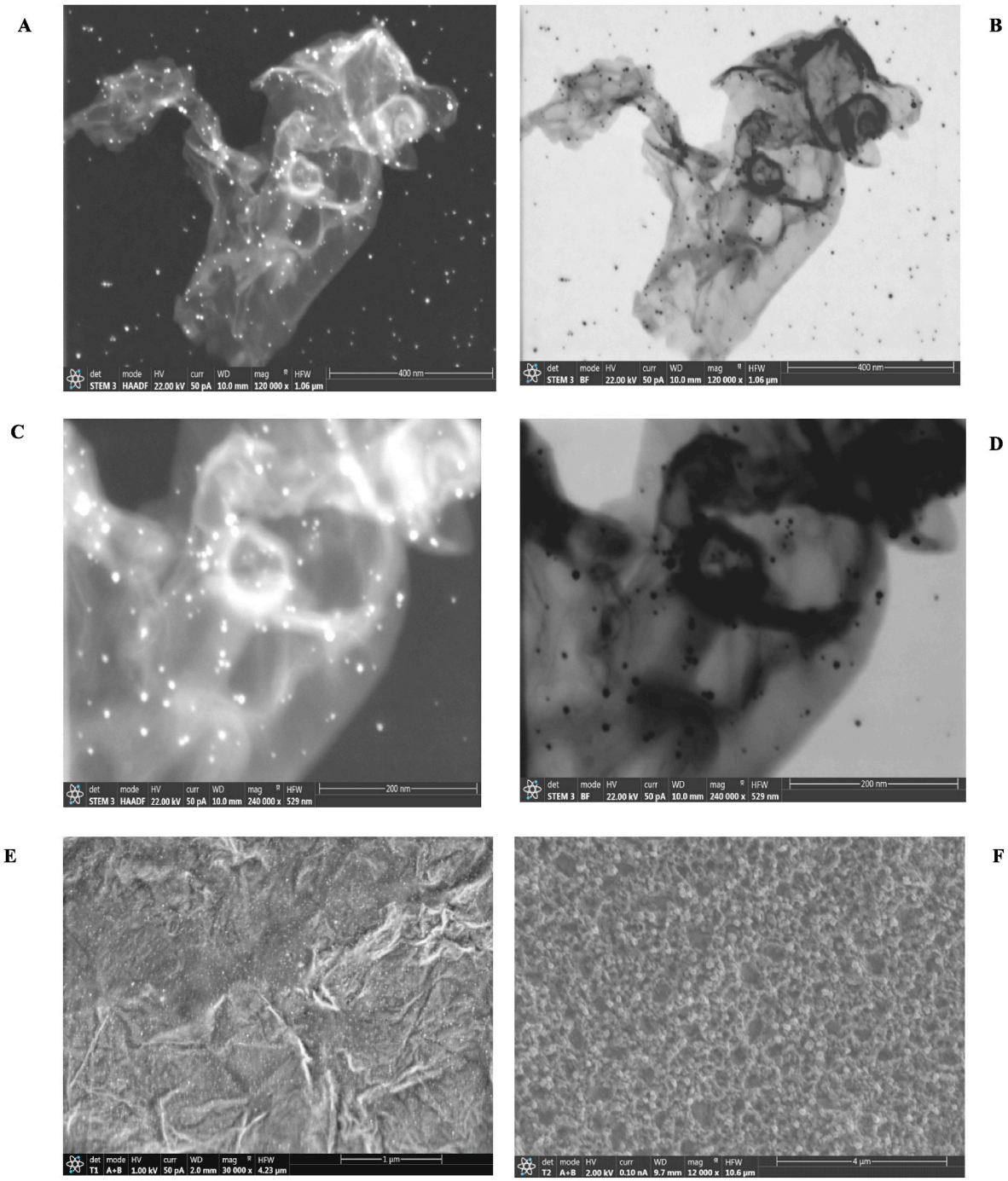

Fig. 2. STEM images of the rGO-Au_{nano} (A–D), and SEM images of the PNA-based sensor before (E) and after (F) the SI-RAFT polymerization.

2.3. Detection process of the SARS-CoV-2 RdRP

During the measurement, the fixed concentration of SARS-CoV-2 RdRP was added inside the disposable well cell to interact with the attached PNA probes for 40 min. After that, the electrode was washed with the running phosphate-buffered saline (PBS, 0.1 M, pH 7.4) to remove any loosely attached target SARS-CoV-2 RdRP. Consequently, the SI-RAFT strategy for the amplification of the signal was done based on the previous report [8], Briefly, 5.0 mM Zr^{4+} solution (prepared with 15% EtOH) was dropped inside a disposable cell and allowed Zr^{4+} ions to interact with the phosphate groups of SARS-CoV-2 RdRP for 15 min at 37 °C. After that, the electrode was washed with DI water several times. After that, 300 μL 0.5 mM CPAD solution (15% EtOH) was drooped inside the disposable cell to interact with the Zr^{4+} ions of the electrode (CSPE/rGO-Au_{nano}/PNA/DNA-Zr_n^{4+}) for 30 min at 37 °C. The electrode was then rinsed several times with DI water containing 15% EtOH. 300 μL of polymerization solution (0.2 mM FcMMA and 2 μM AIPH (free--radical initiator) freshly prepared in 15% DMF) was added inside the disposable cell to generate the poly-FcMMA (poly-redox) for 90 min at 47 °C. Finally, the electrode was washed several times with DI water-15% DMF and the signal was recorded in 0.1 M PBS with the SWV method. Fig. 1 shows the schematic fabrication of the PNA-based sensor and measurement process of the gene target (SARS-CoV-2 RdRP).

The same strategy was applied to study the effect of the interfering gene fragments on the response of the PNA-based sensor.

Since the PNA probe did not have any phosphate group, therefore,

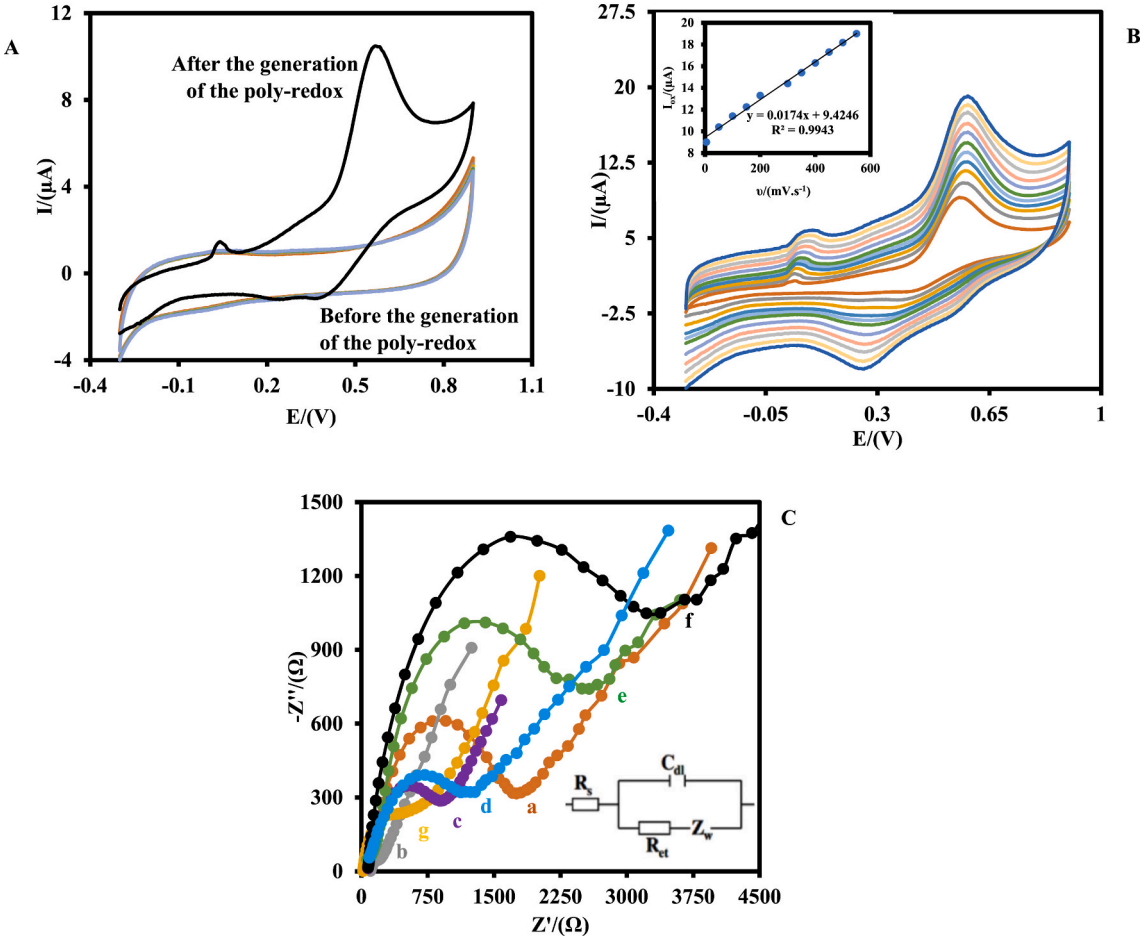

Fig. 3. (A) CV of the electrode before and after the generation of the poly redox at 50 mV s^{-1} in 0.1 M PBS. (B) CVs of the CSPE (a) the CSPE/rGO-Au_{nano} (b) the CSPE/rGO-Au_{nano}/PNA (c), the CSPE/rGO-Au_{nano}/PNA/DNA (d), the CSPE/rGO-Au_{nano}/PNA/DNA/Zr_n^{4+} (e), the CSPE/rGO-Au_{nano}/PNA/DNA/Zr_n^{4+}/CPAD (f), the CSPE/rGO-Au_{nano}/PNA/DNA/Zr_n^{4+}/CPAD/Poly-redox (g) in 0.1 M PBS (pH 7.4) at various scan rates from 5 to 550 mV s^{-1} (5, 50, 100, 150, 200, 300, 350, 400, 450, 500, and 550 from inner to outer). Inset: plot of the oxidation peak current (I_{ox}) versus scan rate (υ). (C) EIS of the in 5 mM $Fe(CN)_6^{3-/4-}$ couple (1:1) and 0.1 M PBS. the Nyquist diagrams. R_s: Solution resistance, R_{ct}: Charge transfer resistance, C_{dl}: Double layer capacitance, Z_w: Warburg impedance. AC amplitude voltage was 10 mV, DC voltage was 0.2 V, and frequency range was 100,000 Hz–0.1 Hz.

Zr^{4+} ions will only attach to SARS-CoV-2 RdRP. As the concentration of the SARS-CoV-2 RdRP increases, more Zr^{4+} ions will attach to the surface of the electrode, and subsequently, more poly-redox will synthesize on the surface of the electrode.

3. Results and discussions

3.1. Characterization of the nanomaterials

Fig. 2 (A-D) shows the STEM images of the rGO-Au_{nano} nanocomposite. As shown, the surface of the fluctuated rGO sheet was decorated with gold nanoparticles with an average size of 9.6 nm. The SEM image of the PNA-based sensor before (E) and after (F) the generation of the poly-redox was also investigated. As can be seen, after the poly-redox generation, plenty of polymer particles on the surface of the PNA-based sensor were generated. The elemental analysis of the electrode after the generation of the poly-redox was also studied (Fig. S4). The result indicated Fe, P, and Zr elements were excess on the surface of the electrode, demonstrating the SI-RAFT process was done successfully.

3.2. Electrochemical characterization of the electrode

Fig. 3A shows the CVs of the step-wise characterization of the electrodes in 0.1 M PBS (pH 7.40). As can be seen, there are not any faradaic currents for the CVs of the CSPE, CSPE/rGO-Au_{nano}, CSPE/rGO-Au_{nano}/PNA, CSPE/rGO-Au_{nano}/PNA/DNA-Zr^{4+}, and CSPE/rGO-Au_{nano}/PNA/DNA-Zr_n^{4+}/CPAD. But after the generation of the poly-redox on the surface of the electrode, an oxidation peak was applied at 0.6 V. It indicates the SI-RAFT polymerization was done on the surface of the electrode. The CVs of the CSPE/rGO-Au_{nano}/PNA/DNA/Zr_n^{4+}/CPAD/Poly-redox were recorded at different scan rates (Fig. 3B). The peak current was linearly proportional to the scan rate (5–550 V s^{-1}) (Fig. 3B inset). It indicated that the poly-redox was an adsorption-controlled process.

The EIS method was also used for the characterization of the electrode in 5 mM $Fe(CN)_6^{3-/4-}$ (Fig. 3C). As shown, the modification of the CSPE with rGO-Au_{nano} composite (b) decreased the charge transfer resistance (R_{ct}) of the CSPE (a). However, after the immobilization of the thiol-terminated PNA probe on the surface of the electrode (c) increased the R_{ct} because of the mass transfer limitation of the PNA probes for $Fe(CN)_6^{3-/4-}$. After the interaction of the SARS-CoV-2 RdRP DNA with PNA (d), the R_{ct} of the electrode was increased because of the electrostatic repulsion interaction between nucleotide bases of aptamer and $Fe(CN)_6^{3-/4-}$ redox probe. The R_{ct} of the electrode was increased as Zr^{4+} (e) and CPAD (f) were attached to the electrode. It can be because of the mass transfer limitation of $Fe(CN)_6^{3-/4-}$ to the surface of the electrode. However, after the generation of the poly-redox on the surface of the electrode (g), the R_{ct} was decreased. The reasonable explanation is that the generation of the poly-

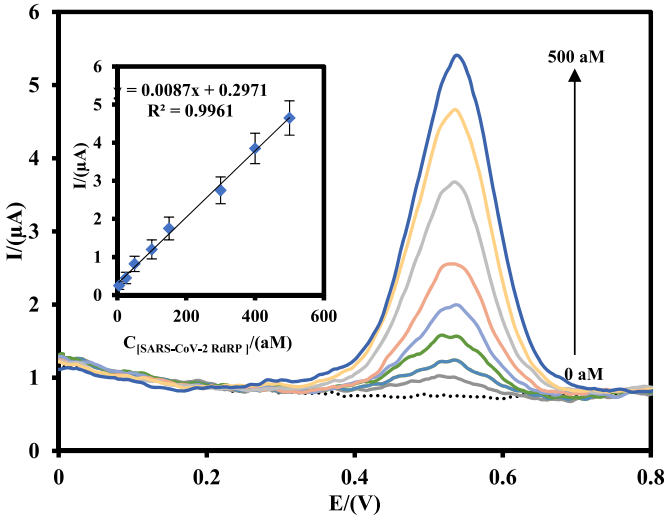

Fig. 4. SWV of the PNA-based sensor for the different concentrations of the SARS-CoV-2 RdRP in 0.1 M PBS. The corresponding calibration plots of SWV response toward SARS-CoV-2 RdRP (0, 5.0, 25.0, 50.0, 100.0, 150.0, 300.0, 400.0, and 500.0 aM) (inset). The error bars were obtained by using four different PNA-based sensors.

redox facilitated the interfacial charge transfer [8,11].

3.3. Voltammetric detection of SARS-CoV-2 RdRP

SWV of the PNA-based sensor for the different concentrations of SARS-CoV-2 RdRP (5–500 aM) is shown in Fig. 4, the peak current was increased as the SARS-CoV-2 RdRP concentration increased. Therefore, based on the change in response mechanism, the proposed measurement strategy is a signal-on method. The response of the PNA-based sensor to SARS-CoV-2 RdRP with a regression equation of I (μA) = 0.008 $C_{SARS\text{-}CoV\text{-}2\ RdRP}$ + 0.297 and coefficient of determination (R^2) of 0.996 (inset of Fig. 4). The limit of detection (LOD) of the PNA-based sensor was calculated to be 0.8 aM (3 × Standard deviation of the blank signal/ Slope of the calibration curve). The analytical performances of the PNA-based sensor have been compared with the previous sensors for SARS-CoV-2 RdRP in Table 1. As can be seen, the LOD of the proposed sensor was lower than the others. It is because of existing the huge amount of redox molecules (poly-redox) on the surface of the sensor. Howevere, the proposed sensor has the longer response time in comperation to the most of the genosensor for SARS-CoV-2 RdRP.

3.4. Selectivity and stability of PNA-based sensor

The selectivity of the PNA-based sensor to 25 aM SARS-CoV-2 RdRP in the presence of the short fragment gene of the H1N1 (25 aM) and MERS-CoV (25 aM) have been investigated (Fig. 5A). During the measurement, 300 μL of a solution containing the same concentration of the SARS-CoV-2 RdRP, the short fragment gene of the H1N1, and MERS-CoV have been added inside the disposable cell that was attached to the PNA-based sensor. After 1 h, the electrode was washed and the process of the SI-RAFT polymerization was done as mentioned before in section 2.3. As can be seen, the response of the proposed sensor to 25 aM SARS-CoV-2 RdRP (a) did not affect by interfering gene fragments of H1N1 (b) and MERS-CoV (c), indicating the high selectivity of the PNA-based sensor to the SARS-CoV-2 RdRP.

The stability of the PNA-based sensor has been studied for 20 days by recording its EIS signal in 5 mM $Fe(CN)_6^{3-/4-}$ and 0.1 M PBS (Fig. 5 B). As can be seen, there are no sensible changes in the EIS of the PNA-based sensor. The reasonable explanation for the high stability of the sensor can be due to using the green synthesized rGO-Au_{nano} composite for the modification of the electrode surface. Because the green synthesized nanocomposites prepare a biocompatible microenvironment for the biomaterials like aptamers [22].

The PNA-based sensor was also applied for the measurement of SARS-CoV-2 RdRP in a human saliva sample. Briefly, 2.0 mL of human saliva sample was filtered to remove any bacterial and other suspended particles which might find in it. Then 90.0 μL of human saliva sample was added to 900.0 μL of PBS (0.1 M, pH 7.4). After that, the solution was mixed with 10.0 μL of SARS-CoV-2 RdRP (5.0 fM) and subsequently, the mixture was transferred into a disposable cell attached to a PNA-based sensor. During this process, the concentration of the SARS-CoV-2 RdRP was diluted from 5 fM to 50 aM. The same measurement process that was mentioned in section 2.3 was applied to generate the poly-redox. Finally, the SWV of the PNA-based sensor to 50 aM of SARS-CoV-2 RdRP was recorded in 0.1 M PBS. This process was repeated 4 times. The results were compared with the polymerase chain reaction (PCR) and reported in Table S3. The recovery of the analysis was found to be 106.5%. The *t*-test and p-test values indicated that there is no significant difference between the responses of the proposed sensor and PCR to 50 aM.

Finally, the reproducibility of the biosensor was investigated with four biosensors (Fig. S5) by using the EIS method. As shown, the semi-circles in the Nyquist plots of the biosensors are the same, indicating the excellent reproducibility of the biosensor.

Table 1
Comparison of the proposed PNA-based sensor with the other genosensors for the viruses.

Sensor	Target	Method	Response range	LOD	Response time	Application	Ref.
DNA tetrahedron entropy-driven ECL biosensor	SARS-CoV-2 RdRP	ECL	1.0 fM–100.0 pM	2.67 fM	45 min	Human serum samples	[19]
Two-dimensional gold nanoislands/DNA	SARS-CoV-2 RdRP	LSPR	0.22 pM–50.0 μM	0.22 pM	<17 min	–	[13]
Silver nanoparticles/PNA	MERS-CoV-DNA	Colorimetry	20.0–1000.0 nM	1.53 nM	–	–	[6]
CPSE/SCX8-RGO/Au@Fe_3O_4/DNA	RNA of SARS-CoV-2	DPV	10 aM−1.0 pM	3 aM	180 min	Various human samples	[20]
Pst-AAm/CdSe/ZnS QDs/DNA and MBs/ DNA	HIV-DNA	ECL	0.05 pM–50.0 nM	39.8 fM	105 min	Various human and animal samples	[21]
CPE-HT18C6(Ag)/chitosan/ SiQDs@PAMAM/DNA	SARS-CoV-2 RdRP	DPV	1.0 pM–8.0 nM	0.3 pM	25 min	Human sputum samples	[14]
CSPE/rGO-Au_{nano}/PNA	SARS-CoV-2 RdRP	SWV	5.0–500.0 aM	0.8 aM	135 min	Human saliva samples	This work

ECL: Electrochemiluminescence; LSPR: Localized surface plasmon resonance; Pst-AAm: Poly(styrene/acrylamide) nanospheres; MBs: Magnetic nanobeads; SCX8-RGO: P-sulfocalix [8]arene (SCX8) functionalized graphene; Au@Fe_3O_4: Gold nano particels decorated magnetic nanoparticles; QDs: Quantum dot; DPV: Differential pulse voltammetry; HT18C6: Silver ions (Ag^+) in the hexathia-18-crown-6; CPE: Carbon paste electrode; SiQDs@PAMAM: PAMAM dendrimer-coated silicon quantum dots.

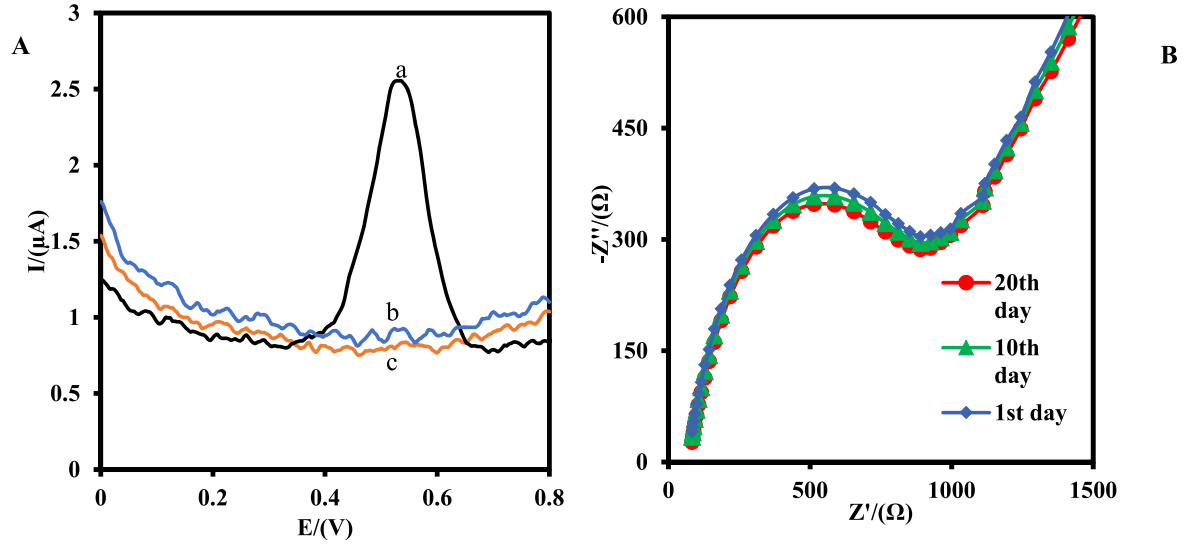

Fig. 5. (A) Selectivity of the PNA-based sensor to 25 aM SARS-CoV-2 RdRP in the presence of the short fragment gene of the 25 aM H1N1 (b) and 25 aM MERS-CoV (c) in 0.1 M PBS. (B). Stability of the Nyquist plots of the PNA-based sensor during 20 days. The Nyquist plots were recorded in 5 mM $Fe(CN)_6^{3-/4-}$ couple (1:1) and 0.1 M PBS. AC amplitude voltage was 10 mV, DC voltage was 0.2 V, and frequency range was 100 kHz-0.1 Hz.

4. Conclusions

In summary, a PNA-based sensor has been developed to detect the SARS-CoV-2 RdRP. Meanwhile, the signal of the sensor was amplified by generating the poly-FcMMA via the SI-RAFT method on the surface of the electrode. Notably, the proposed PNA-based sensor could detect the SARS-CoV-2 RdRP in the range of 5–500 aM with a LOD of 0.8 aM. It also showed high selectivity to the SARS-CoV-2 RdRP in the presence of the MERS-CoV and H1N1 gene fragments and high stability after 20 days. Overall, a promising detection technique has been proposed for the detection of COVID-19 in its early stages, which helps decrease economic losses and fatalities. However, the response time of the proposed sensor is higher than the most of the previous sensor for SARS-CoV-2 RdRP.

Credit author statement

Mahmoud Amouzadeh Tabrizi: Conceptualization, Methodology, Data curation, Formal analysis, Validation, Investigation, Visualization, Writing – original draft, Resources, Project administration, Funding acquisition.

Declaration of competing interest

The authors declare that they have no known competing financial interests or personal relationships that could have appeared to influence the work reported in this paper.

Data availability

Data will be made available on request.

Acknowledgments

This project has received funding from the European Union's Horizon 2020 research and innovation program under the Marie Sklodowska-Curie grant agreement No 801538.

Appendix A. Supplementary data

Supplementary data to this article can be found online at https://doi.org/10.1016/j.talanta.2023.124490.

References

[1] K.Y. Goud, K.K. Reddy, M. Satyanarayana, S. Kummari, K.V. Gobi, A review on recent developments in optical and electrochemical aptamer-based assays for mycotoxins using advanced nanomaterials, Microchim. Acta 187 (2019) 29.
[2] Y. Yang, W. Li, J. Liu, Review of recent progress on DNA-based biosensors for Pb2+ detection, Anal. Chim. Acta 1147 (2021) 124–143.
[3] D. Kong, X. Wang, C. Gu, M. Guo, Y. Wang, Z. Ai, S. Zhang, Y. Chen, W. Liu, Y. Wu, C. Dai, Q. Guo, D. Qu, Z. Zhu, Y. Xie, Y. Liu, D. Wei, Direct SARS-CoV-2 nucleic acid detection by Y-shaped DNA dual-probe transistor assay, J. Am. Chem. Soc. 143 (2021) 17004–17014.
[4] Z. Hatami, F. Jalali, M. Amouzadeh Tabrizi, M. Shamsipur, Application of metal-organic framework as redox probe in an electrochemical aptasensor for sensitive detection of MUC1, Biosens. Bioelectron. 141 (2019), 111433.
[5] M. Amouzadeh Tabrizi, M. Shamsipur, R. Saber, S. Sarkar, Isolation of HL-60 cancer cells from the human serum sample using MnO2-PEI/Ni/Au/aptamer as a novel nanomotor and electrochemical determination of thereof by aptamer/gold nanoparticles-poly(3,4-ethylene dioxythiophene) modified GC electrode, Biosens. Bioelectron. 110 (2018) 141–146.
[6] P. Teengam, W. Siangproh, A. Tuantranont, T. Vilaivan, O. Chailapakul, C. S. Henry, Multiplex paper-based colorimetric DNA sensor using pyrrolidinyl peptide nucleic acid-induced AgNPs aggregation for detecting MERS-CoV, MTB, and HPV oligonucleotides, Anal. Chem. 89 (2017) 5428–5435.
[7] A. Bini, S. Centi, S. Tombelli, M. Minunni, M. Mascini, Development of an optical RNA-based aptasensor for C-reactive protein, Anal. Bioanal. Chem. 390 (2008) 1077–1086.
[8] Q. Hu, D. Han, S. Gan, Y. Bao, L. Niu, Surface-initiated-reversible-addition–fragmentation-chain-transfer polymerization for electrochemical DNA biosensing, Anal. Chem. 90 (2018) 12207–12213.
[9] Q. Hu, Y. Luo, X. Cao, Z. Chen, Y. Huang, L. Niu, Bioinspired electro-RAFT polymerization for electrochemical sensing of nucleic acids, ACS Appl. Mater. Interfaces 13 (2021) 54794–54800.
[10] H. Sun, J. Kong, Q. Wang, Q. Liu, X. Zhang, Dual signal amplification by eATRP and DNA-templated silver nanoparticles for ultrasensitive electrochemical detection of nucleic acids, ACS Appl. Mater. Interfaces 11 (2019) 27568–27573.
[11] Q. Hu, L. Su, Y. Luo, X. Cao, S. Hu, S. Li, Y. Liang, S. Liu, W. Xu, D. Qin, L. Niu, Biologically mediated RAFT polymerization for electrochemical sensing of kinase activity, Anal. Chem. 94 (2022) 6200–6205.
[12] J. Zhang, Y. Ba, Q. Liu, L. Zhao, D. Wang, H. Yang, J. Kong, CuBr(2)/EDTA-mediated ATRP for ultrasensitive fluorescence detection of lung cancer DNA, J. Adv. Res. 22 (2020) 77–84.
[13] G. Qiu, Z. Gai, Y. Tao, J. Schmitt, G.A. Kullak-Ublick, J. Wang, Dual-functional plasmonic photothermal biosensors for highly accurate severe acute respiratory syndrome coronavirus 2 detection, ACS Nano 14 (2020) 5268–5277.

[14] L. Farzin, S. Sadjadi, A. Sheini, E. Mohagheghpour, A nanoscale genosensor for early detection of COVID-19 by voltammetric determination of RNA-dependent RNA polymerase (RdRP) sequence of SARS-CoV-2 virus, Microchim. Acta 188 (2021) 121.
[15] M. Amouzadeh Tabrizi, A. Tavakkoli, V. Dhand, K.Y. Rhee, S.-J. Park, Eco-friendly one-pot synthesis of gold decorated reduced graphene oxide using beer as a reducing agent, J. Ind. Eng. Chem. 20 (2014) 4327–4331.
[16] A. Dalal Ravina, P.S. Gill, J. Narang, M. Prasad, H. Mohan, Genosensor for rapid, sensitive, specific point-of-care detection of H1N1 influenza (swine flu), Process Biochem 98 (2020) 262–268.
[17] M.M. Walczak, D.D. Popenoe, R.S. Deinhammer, B.D. Lamp, C. Chung, M.D. Porter, Reductive desorption of alkanethiolate monolayers at gold: a measure of surface coverage, Langmuir 7 (1991) 2687–2693.
[18] X. Yiwei, Z. Wen, H. Xiaowei, S. Jiyong, Z. Xiaobo, L. Yanxiao, C. Xueping, H. E. Tahir, L. Zhihua, A self-assembled L-cysteine and electrodeposited gold nanoparticles-reduced graphene oxide modified electrode for adsorptive stripping determination of copper, Electroanalysis 30 (2018) 194–203.
[19] Z. Fan, B. Yao, Y. Ding, J. Zhao, M. Xie, K. Zhang, Entropy-driven amplified electrochemiluminescence biosensor for RdRp gene of SARS-CoV-2 detection with self-assembled DNA tetrahedron scaffolds, Biosens. Bioelectron. 178 (2021), 113015.
[20] H. Zhao, F. Liu, W. Xie, T.-C. Zhou, J. OuYang, L. Jin, H. Li, C.-Y. Zhao, L. Zhang, J. Wei, Y.-P. Zhang, C.-P. Li, Ultrasensitive supersandwich-type electrochemical sensor for SARS-CoV-2 from the infected COVID-19 patients using a smartphone, Sens. Actuators B Chem. 327 (2021), 128899.
[21] Z. Wu, F. Luo, W. Wen, X. Zhang, S. Wang, Enrichment–stowage–cycle strategy for ultrasensitive electrochemiluminescent detection of HIV-DNA with wide dynamic range, Anal. Chem. 91 (2019) 12238–12245.
[22] M. Amouzadeh Tabrizi, M. Shamsipur, R. Saber, S. Sarkar, Simultaneous determination of CYC and VEGF165 tumor markers based on immobilization of flavin adenine dinucleotide and thionine as probes on reduced graphene oxide-poly (amidoamine)/gold nanocomposite modified dual working screen-printed electrode, Sens. Actuators B Chem. 240 (2017) 1174–1181.